Title

Controlled Single-Electron Transfer via Metal—Ligand Cooperativity Drives Divergent Nickel-Electrocatalyzed Radical Pathways

Journal

Journal of the American Chemical Society, 143(18)

ISSN

0002-7863

Authors

Wuttig, Anna
Derrick, Jeffrey S
Loipersberger, Matthias
et al.

Publication Date

2021-05-12

DOI

10.1021/jacs.1c01487

Peer reviewed

Controlled Single Electron Transfer via Metal-Ligand Cooperativity Drives Divergent Nickel Electrocatalyzed Radical Pathways

Anna Wuttig,[†] Jeffrey S. Derrick,[†] Matthias Loipersberger,[‡] Andrew Snider,[‡] Martin Head-Gordon,[‡,§] Christopher J. Chang,*[†,§,Δ] F. Dean Toste*,[†,§]

[†]Department of Chemistry, University of California, Berkeley, California, U.S.A.
[‡]Pitzer Center for Theoretical Chemistry, Department of Chemistry, University of California, Berkeley, California, U.S.A.
[Δ]Department of Molecular and Cell Biology, University of California, Berkeley, California, U.S.A.
[§] Chemical Sciences Division, Lawrence Berkeley National Laboratory, Berkeley, California, USA

ABSTRACT: Electrocatalysis enables the construction of C–C bonds under mild conditions via controlled formation of carbon-centered radicals. For sequences initiated by alkyl halide reduction, coordinatively-unsaturated Ni complexes commonly serve as single electron transfer agents, giving rise to the foundational question of whether outer- or inner-sphere electron transfer oxidative addition prevails in redox mediation. Indeed, rational design of electrochemical processes requires the discrimination of these two electron transfer pathways, as they can have outsized effects on the rate of substrate bond activation and thus impact radical generation rates and downstream product selectivities. We present results from combined synthetic, electroanalytical, and computational studies that examine the mechanistic differences of single electron transfer to alkyl halides imparted by Ni metal-ligand cooperativity. Electrogenerated reduced Ni species, stabilized by delocalized spin density onto a redox-active tpyPY2Me polypyridyl ligand, activates alkyl iodides via outer-sphere electron transfer, allowing for the selective activation of alkyl iodide substrates over halogen atom donors and the controlled generation and sequestration of electrogenerated radicals. In contrast, the Ni complex possessing a redox-innocent pentapyridine congener activates the substrates in an inner-sphere fashion owning to a purely metal-localized spin, thereby activating both substrates and halogen atom donors in an indiscriminate fashion, generating a high concentration of radicals and leading to unproductive dimerization. Our data establish that controlled electron transfer via Ni-ligand cooperativity can be used to limit undesired radical recombination products and promote selective radical processes in electrochemical environments, providing a generalizable framework for designing redox mediators with distinct rate and potential requirements.

INTRODUCTION

The controlled formation of carbon-centred radicals facilitates the construction of value-added products. While it is well-established that these open-shell intermediates are readily accessed via halogen atom transfer from alkyl halide (RX) feedstocks,[1–4] the toxicity of tin, silicon, or trialkylborane reagents traditionally employed to initiate this reactivity motivates the development of complementary synthetic methods with improved sustainability. Among the numerous alternatives pursued,[5,6,7–14,15,16] strategies that enable RX activation via single electron transfer (SET) present an opportunity for radical generation to be interfaced with SET catalysts, where energy input from visible light[17] or electricity[18,19] enables turnover under mild conditions. RX reduction under photoredox conditions typically employ coordinatively-saturated Rh or Ir polypyridyl catalysts.[8–10,12,20,21] In these systems, it is hypothesized that initial light sensitization steps form reductants that activate substrates via outer-sphere electron transfer (OSET).[22,23] Thus, the interaction of the starting material with the metal center, promoting an inner-sphere electron transfer (ISET) event, or coordination of the ensuing carbon-centred radical is not invoked. Hence, the photocatalyst ligand is tuned to optimize the redox potential necessary to facilitate the OSET step.[8,9,12] In contrast, for electrosynthetic sequences initiated by RX reduction, coordinatively unsaturated Ni complexes possessing diverse ligand scaffolds commonly serve as SET agents,[24–26] giving rise to the question of whether OSET or ISET oxidative addition prevails in catalytic redox mediation. Moreover, the design of more complex electrochemical radical processes requires an understanding of the ligand design criteria necessary to direct outer-sphere vs inner-sphere redox reactivity, as these distinct electron transfer reaction pathways are expected to lead to dramatic differences in the rate of RX bond activation near the electroactive interface[27] and thereby impact radical production rates and downstream product selectivity.

Studies suggest that Ni ligand tuning directs both outer-sphere and inner-sphere electron transfer reactivity manifolds towards RX activation. Reported electrosynthetic reaction sequences imply that electrogenerated Ni(I) complexes reduce RX via OSET, thereby regenerating Ni(II) for subsequent turnover.[28,29] Indeed, ligand tuning by both redox-active and redox-inactive tetradentate ligands has been shown to alter the redox potential for Ni(II)/Ni(I) by over 1 V,[24,25,28,29] and this sole property has been utilized to choose a suitable redox mediator for RX activation prior to direct substrate reduction at more negative potentials.[26] However, it has been shown that Ni complexes span-

ning ~0.8 V can still mediate the reduction of the same RX substrate,[30,31] suggesting that select Ni-based redox mediators may operate, instead, via ISET mechanisms. Indeed, evidence suggests that metal-centered reduction may facilitate ISET pathways towards RX activation. It has been shown that RX oxidative addition processes at Ni(I) complexes bearing a strongly sigma-donating and redox-inactive ligand, i.e. bisphosphine, proceed via an inner-sphere pathway of metal-centered halogen atom abstraction.[32] Similarly, Ni(I) cyclam or tetramethylcyclam, a widely utilized redox mediator for RX reduction[30,33–36] bearing no redox-active ligand, has been shown to catalyze the electroreduction of RX at potential values ~ 1 V more positive than the direct reduction of the substrate, rendering an OSET mechanism unlikely[37]. Yet, the nature of the oxidative addition adduct, i.e. halogen atom transfer[38] vs. two-electron oxidative insertion into the RX bond[39,40], remain unresolved. In addition, Ni(II) Salen complexes with aliphatic imine bridges, exhibit metal-based SET reduction by EPR and UV-vis studies,[41] and inner-sphere reactivity of the corresponding Ni(I) species have been implicated towards RX reduction.[37,42–44] Thus, despite the central role of SET processes in facilitating carbon-centered radical formation in electrochemical environments, the diversity of explored Ni ligand platforms precludes systematic studies of metal-centered reduction on SET, limiting the ability to design more complex electrocatalytic radical processes.

In order to isolate and study the effect of metal-centered reduction on SET to RX, and thereby electrocatalytic carbon-centered radical generation and downstream reactivity, we reasoned that an ideal ligand set requires: (1) a chelating ligand that favors one open metal coordination site to isolate single-electron reactivity over traditional three-centered concerted two-electron oxidative addition pathways; and (2) fine-tuned control over the localization of spin density between the metal center and/or low-ligand ligand orbitals. In this context, recent studies on Fe complexes demonstrate that the incorporation of a pentadentate, redox-active pentapyridine ligand (tpyPY2Me = 6-(1,1-di(pyridin-2-yl)ethyl)-2,2′:6′,2″-terpyridine) shifts electron density away from metal orbitals relative to complexes possessing a redox-innocent pentapyridine congener (PY5Me2 = 2,6-bis(1,1-bis(2-pyridyl)ethyl)pyridine) and can be exploited for electrocatalysis.[45] Thus, the tpyPY2Me and PY5Me2 ligand platforms present an ideal pair to interrogate (1) and (2). Translation of these design elements towards the study of electrocatalyzed RX activation, however, requires the preparation of Ni complexes as the Fe variants are not sufficiently reducing[45] to act as SET redox mediators towards RX reduction.

Here, we report the synthesis and characterization of Ni complexes of tpyPY2Me and PY5Me2 and compare their electrocatalytic performance for RX activation. We combine electrokinetic and bulk electrolysis studies with structural insight from DFT calculations to formulate a mechanistic model that describes the structure of the electroactive reduced complexes and the rate-limiting alkyl iodide (RI) activation processes for both. We find that electrogenerated reduced Ni species, stabilized by delocalized spin density onto the redox-active tpyPY2Me ligand, activates RI via OSET, followed by rapid sequestration of an ensuing radical to furnish an overall bimolecular oxidative addition step. In contrast, the redox-innocent ligand congener, with a purely metal-localized reduction, activates RI at 3-5 orders of magnitude higher rate by ISET, thus leading to uncontrolled free radical formation. We exploit these divergent SET pathways for RI activation in the context of radical cyclization following carboiodination,[46] showing that Ni-ligand cooperativity limits undesired radical recombination products and promotes a selective radical process. More broadly, these findings establish metal-ligand cooperativity as a design element that can be employed to control the rate of electrochemical radical generation and downstream radical reactivity.

RESULTS AND DISCUSSION

Synthesis and Characterization of Ni Complexes. The [Ni(tpyPY2Me)(MeCN)]$^{2+}$, [**Ni-1**]$^{2+}$, complex was synthesized

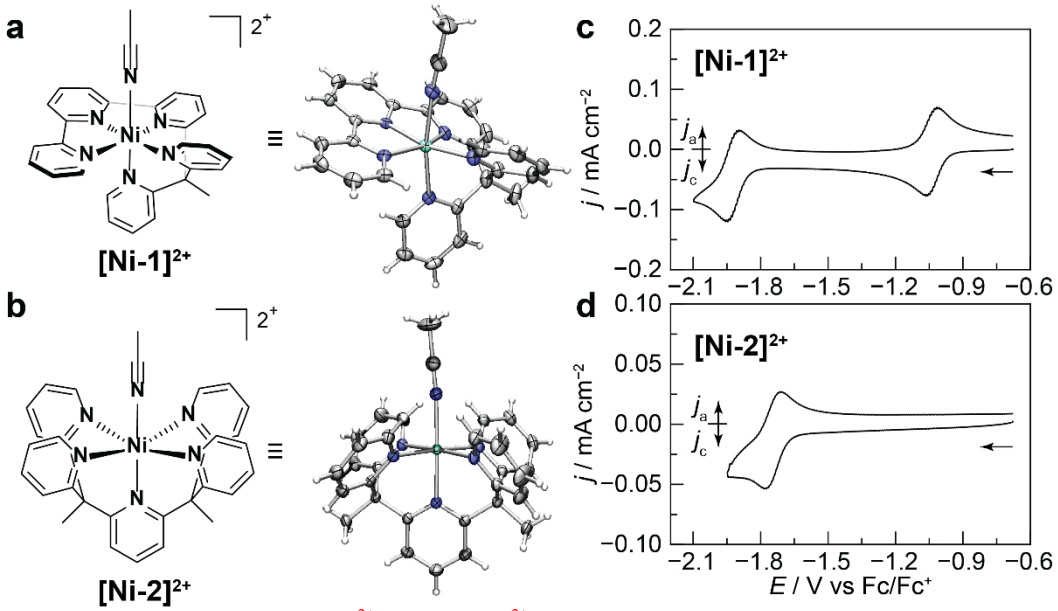

Figure 1. Structures and crystal structures of [**Ni-1**]$^{2+}$ (**a**) and [**Ni-2**]$^{2+}$ determined by single crystal x-ray diffraction (**b**). Thermal ellipsoids are plotted at 50% and 75% probability level for [**Ni-1**]$^{2+}$ and [**Ni-2**]$^{2+}$, respectively. Turquoise, dark blue, and gray ellipsoids signify Ni, N, and C atoms, respectively. Noncoordinating solvent and anions omitted for clarity. Cyclic voltammogram (CV) of 1.8 mM [**Ni-1**]$^{2+}$ (**c**) and 1.4 mM [**Ni-2**]$^{2+}$ (**d**) at 100 mV s^{-1} taken in 0.1 M $TBAPF_6$ in DMF, where CV scans were initiated cathodically from the open circuit potential (–0.68 V vs Fc/Fc^+).

by adopting slight modifications to the literature-reported methods for the analogous iron complex (experimental methods provided in the Supporting Information).[45] In order to elucidate the role of the redox-active tpyPY2Me ligand on redox mediation, the redox-inactive congener, $[Ni(PY5Me2)(MeCN)]^{2+}$, [**Ni-2**]$^{2+}$, was prepared by modifying literature-reported methods for the syntheses of metal complexes bearing the PY5Me2 ligand [47–52]. The solid-state structures of both complexes were characterized by single-crystal x-ray diffraction. In the primary coordination sphere, both [**Ni-1**]$^{2+}$ (**Figure 1a** and **Table S1**) and [**Ni-2**]$^{2+}$ (**Figure 1b** and **Table S2**) adopt a *pseudo*-octahedral structure. The enhanced rigidity of the tpyPY2Me framework gives rise to increased distortion away from an idealized octahedral symmetry relative to the PY5Me2, consistent with observations using Fe.[45] Definitive determination of the structure in solution is precluded by the observation of broad ^{1}H NMR signals, suggesting that both Ni(II) complexes are paramagnetic. Measurements of the effective magnetic moment by the Evans Method confirm this hypothesis; values of 3.2 and 3.0 μ_B (S = 1) are estimated for [**Ni-1**]$^{2+}$ and [**Ni-2**]$^{2+}$, respectively, **Figures S1** and **S2**. Together, these data evince the formation of the desired Ni(II) complexes in which the two high-lying d orbitals, $d_{x^2-y^2}$ and d_{z^2}, are singularly occupied in the ground state.

The [**Ni-1**]$^{2+}$ complex exhibit two redox features while [**Ni-2**]$^{2+}$ exhibits a single feature over the same potential range. **Figure 1c** shows the cyclic voltammogram (CV) of [**Ni-1**]$^{2+}$ taken in 0.1 M $TBAPF_6$ in DMF at 100 mV s^{-1} initiated at the open circuit potential (–0.68 V). Two redox features are observed at $E_{1/2}$ values of –1.92 V (all potentials quoted vs Fc/Fc^+) and –1.04 V. Scan-rate dependent CV measurements, **Figure S3**, reveal that the observed 60 mV separation (ΔE_p) between the peak potential of the anodic and cathodic features persists for both redox events. This observation is characteristic of Nernstian SETs to solution-dissolved reactants,[53] supporting the reversibility, and thus fast ET kinetics, of the redox events associated with [**Ni-1**]$^{2+}$ reduction. Bulk electrolysis measurements of [**Ni-1**]$^{2+}$ conducted at –2.04 V consume 2 F mol^{-1}, **Figure S4**, are in line with the assignment of two redox events, i.e. sequential formation of [**Ni-1**]$^+$ and [**Ni-1**], accessible at this potential. In contrast, the [**Ni-2**]$^{2+}$ complex exhibits a single redox feature with slower ET kinetics. **Figure 1d** displays the CV of [**Ni-2**]$^{2+}$ taken over a similar potential range as [**Ni-1**]$^{2+}$. A redox feature is observed at an $E_{1/2}$ value equalling –1.75 V (**Figure 1d**). As the scan rate is increased, the peak-to-peak separation between the anodic and cathodic features increases, (**Figure S5**), revealing that redox event is influenced by the kinetics of the electron transfer process.[1,3] Determination of the diffusion coefficient of [**Ni-2**]$^{2+}$ (5×10^{-6} cm^2 s^{-1}) by electroanalytical methods (**Figure S5**) allows for the estimation of the electron transfer rate constant, $k_{s,\,[Ni\text{-}2]^{2+}} = 1.1\times10^{-2}$ cm s^{-1}, for forming the reduced [**Ni-2**]$^+$ species, in contrast to the Nernstian behaviour observed for [**Ni-1**]$^{2+}$. The voltammetry results demonstrate that reduced [**Ni-1**], and [**Ni-2**]$^+$ complexes are accessible within 170 mV of one another.

Single-Electron Activation of Alkyl Iodide Substrates by [Ni-1]. To investigate the electrocatalytic reactivity of synthesized [**Ni-1**]$^{2+}$ and [**Ni-2**]$^{2+}$, we screened various alkyl halide substrates to identify variants that were electrochemically activated by both complexes and gave rise to mechanistically distinguishable reactivity. We found that both an activated RI substrate, dimethyl 2-butyl-2-(iodomethyl)malonate (**3**), and less activated RI substrated, cycloiodohexane (CyI), fit this criteria. With these substrates in hand, we studied the catalysts' mechanism of action by employing electroanalytical studies to track the *in-situ* formation and consumption of the reduced forms of [**Ni-1**]$^{2+}$ and [**Ni-2**]$^{2+}$ and combining these insights with bulk electrolysis reactivity studies.

The electrogenerated [**Ni-1**] complex activates **3** in a bimolecular fashion. **Figure 2a** depicts the CV of 1.1 mM [**Ni-1**]$^{2+}$ taken in 0.1 M $TBAPF_6$ in DMF in the absence (black solid trace) and presence of 12 mM of **3** (red solid trace). Upon the addition of **3**, the wave corresponding to [**Ni-1**]$^+$/[**Ni-1**] becomes irreversible and an increase in the cathodic peak current (j_p) relative to the current in the absence of substrate (j_0) is observed. The j_p increases together with the concentration of added **3** up to two electrons ($j_p/j_0 = 2$), **Figure S6a**. This observation suggests that two equivalents of [**Ni-1**] are involved in activating **3**. Bulk electrolysis measurements of equimolar [**Ni-1**]$^{2+}$ and **3** conducted at –2.08 V are consistent with this hypothesis; this process consumes 3 F mol^{-1} (**Figure S7**) in agreement with the assignment of the combined one-electron stoichiometry at the [**Ni-1**]$^{2+}$/[**Ni-1**]$^+$ wave and the two-electron stoichiometry at the [**Ni-1**]$^+$/[**Ni-1**] wave in the presence of **3**. Furthermore, electrochemical studies in the absence of added [**Ni-1**]$^{2+}$ failed to activate **3** at the same potential, consistent with the assignment of [**Ni-1**] as the active redox mediator. The peak potential (E_p) for the direct reduction of **3** is –2.52 V (**Figure S8a**); a value that is 0.58 V more negative than the E_p of **3** activation in the presence of [**Ni-1**] (–1.94 V; **Figure 2a**). This observation rules out competing direct reduction pathways of **3** since they are not electrochemically accessible at the potential values examined. A mechanistic sequence compatible with these observations is the following,

$$[\mathbf{Ni\text{-}1}]^{2+} + e^- \rightleftharpoons [\mathbf{Ni\text{-}1}]^+ \quad (1)$$

$$[\mathbf{Ni\text{-}1}]^+ + e^- \rightleftharpoons [\mathbf{Ni\text{-}1}] \quad (2)$$

$$[\mathbf{Ni\text{-}1}] + RI \xrightarrow{k_1} R\bullet + I^- + [\mathbf{Ni\text{-}1}]^+ \quad (3)$$

$$[\mathbf{Ni\text{-}1}] + R\bullet \xrightarrow{k_r} [(\mathbf{Ni\text{-}1})(R)] \quad (4)$$

where k_1 is the rate constant of the homogeneous single electron transfer between [**Ni-1**] and **3** (denoted above as a general alkyl iodide, RI) and k_r is the rate constant associated with rapid rebound of the resultant radical (R•) to [**Ni-1**]. This proposed sequence captures the two redox features observed for [**Ni-1**]$^{2+}$ (steps 1 and 2) and the two-electron stoichiometry at the [**Ni-1**]$^+$/[**Ni-1**] wave observed in the presence of **3** (steps 3 and 4). Electrochemical simulations provide further support of this hypothesis. By assuming that step 1 does not play a role in substrate activation other than accessing the redox potential necessary to form [**Ni-1**]$^+$, steps 2 to 4 can be described using the well-established theoretical framework of homogeneous redox catalysis in which a reactive intermediate (here, R•) rapidly adds to the catalyst active form (here, [**Ni-1**]) following a rate-determining substrate activation event.[54,55] This mechanistic framework permits the construction of working curves, which relate theoretical j_p/j_0 values to the ratio of the substrate and catalyst concentration (here, $C_{RI}/C_{[Ni\text{-}1]^{2+}}$).[54,55] However, the electrochemical response of [**Ni-1**] in the presence of **3**, is convoluted by the observation of a broad capacitive feature ($E < –1.54$ V) and possible tail of an overlapping reductive feature ($E < –2.08$ V) as the concentration of **3** increases (**Figures 2a** and **S6a**). For these reasons, incremental changes in j_p/j_0 are not suit-

able observables to compare against theory. Therefore, theoretical working curves depicting predicted shifts in E_p were constructed, see **Figure S6c** and the SI for the procedure, predicting an anodic shift in E_p as the kinetic parameter increases. Comparison of the experimental E_p values with the working curves established for varying $C_{RI}/C_{[Ni\text{-}1]^{2+}}$ values (**Figure S6c**) leads to an estimation of k_1 (log k_1 = 2.841±0.007 [M^{-1} s^{-1}]), **Table S3** and **Figure 2c** (labeled red circle). We observe agreement of k_1 values estimated at varying scan rates (**Figure S6b** and **Table S3)** providing further support of the proposed mechanistic sequence. This mechanism is in line with reports that expose the role of other one-electron reductants, e.g. $KCo(CN)_5^{3-}$, $KM(CO)_5$ (M = Mn, Re), and [Ni(1R,4R,8S,11S-tetramethylcyclam)]$^+$,[38,56–58] in similarly facilitating bimolecular oxidative addition pathways of polar reagents. Together, these data support a bimolecular oxidative addition pathway of **3** by electrogenerated [**Ni-1**].

The [**Ni-1**] complex activates CyI at a lower rate than **3**. **Figure 2b** shows the CV of 1.1 mM [**Ni-1**]$^{2+}$ in the absence (black solid trace) and presence of 11 mM of CyI (blue solid trace). We observe: (1) increased current density at the redox couple associated with [**Ni-1**] formation; (2) j_p/j_0 approaching a value of 2 as the CyI concentration is increased (**Figure S9a**); and (3) direct CyI reduction at E values 580 mV more negative than in the presence of [**Ni-1**], **Figure S8b**. Comparison of the experimental E_p values with the identical working curve utilized to analyze the activation of **3** (*vide supra*) (**Figure S9c**) leads to an estimation of k_1 (log k_1 = 2.12±0.04 [M^{-1} s^{-1}]), **Table S3** and **Figure 2c** (labeled blue square). We observe agreement of k_1 values estimated at varying scan rates (**Figure S9b** and **Table S3**) providing further support of the mechanistic sequence, steps 2 through 4. Together, these data suggest that electrogenerated [**Ni-1**] activates CyI in a similar manner as **3**, however, at a 5-fold slower rate.

To distinguish the mechanism of the homogeneous ET step involved in substrate activation by [**Ni-1**], *i.e.* step 3 in the proposed sequence, we compared estimated k_1 values with those obtained for **3** and CyI activation by a series of aromatic redox mediators (Ar). As there is no metal center on the electrogenerated aromatic radical anion (Ar•$^-$) to facilitate an inner-sphere interaction with the substrate, the experimentally determined rate of ET between Ar•$^-$ and RI (k_1 in step 3 of the proposed sequence, where Ar•$^-$ replaces the Ni complex) represents values expected for a purely outer-sphere homogeneous electron transfer event (OSET). Thus, estimated k_1 values are expected to be proportional to the activation free energy, which is lowered by increases in the driving force, *i.e.* the difference of $E_{1/2}$ of varying Ar from the fixed standard potential of RI/R• + I^- couple (approximately –1.7 V for 1-iodobutane)[55] by the Hush-Marcus relationship.[59–61] Establishing this relationship for the substrates examined in this study serves as a diagnostic method[27,62,63] to identify if [**Ni-1**] similarly activates RI in an OSET fashion. The aromatic compounds, **4-10** in **Figure 2c**, were judiciously chosen as precursors for electrogenerated Ar•$^-$. First, their $E_{1/2}$ values span a 400 mV potential range that closely overlaps with that of [**Ni-1**]$^+$/[**Ni-1**]. Second, after screening several literature-reported aromatic redox mediators,[27,55] we narrowed the selection to **4-10** due to their well-

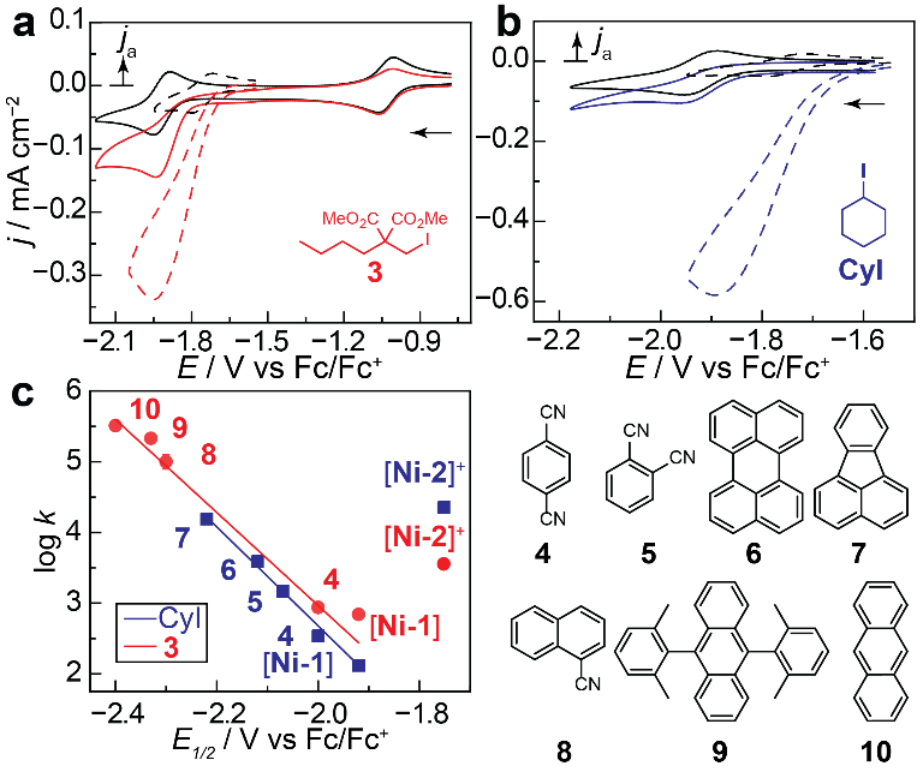

Figure 2. (**a**) CV of 1.1 mM [**Ni-1**]$^{2+}$ in the absence (solid black) and presence (solid red) of 12 mM **3**. CV of 0.9 mM [**Ni-2**]$^{2+}$ in the absence (dashed black) and presence (dashed red) of 10 mM **3**. (**b**) CV of 1.1 mM [**Ni-1**]$^{2+}$ in the absence (solid black) and presence (solid blue) of 11 mM CyI. CV of 1.0 mM [**Ni-2**]$^{2+}$ in the absence (dashed black) and presence (dashed blue) of 11 mM CyI. CVs collected at 100 mV s^{-1} in 0.1 M $TBAPF_6$/DMF, where CV scans were initiated in the cathodic direction. (**c**) Variation in the estimated rate constant of the rate-determining step of **3** (red) and CyI (blue) activation with the redox potential of investigated Ni complexes or aromatic anions **4-10**. Straight line by regression for **3** activation by **10** to [**Ni-1**], R^2 = 0.995 and for CyI activation by **7** to [**Ni-1**], R^2 = 0.998. The data points are larger than the error bars in estimated k.

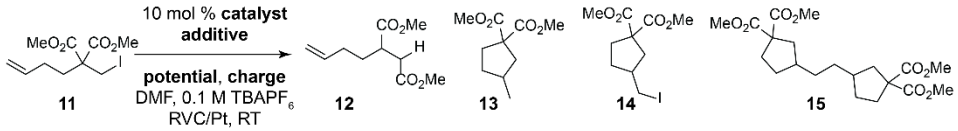

entry	catalyst	additive	F mol^{-1}	V vs Fc/Fc$^+$	12	13	14	15
a	none	none	2	−2.73 V	50(30)*	nd	nd	nd
b	[**Ni-1**]$^{2+}$	none	1	−2.03 V	nd	31	17	nd
c	e-[**Ni-1**]	none	none	none	nd	<4%	nd	nd
d	[**Ni-1**]$^{2+}$	NaOTf	1	−2.03 V	nd	nd	nd	46(30)*
e	[**Ni-1**]$^{2+}$	CyI	1	−2.03 V	nd	19	75(40)*	nd
f	[**Ni-2**]$^{2+}$	none	1	−1.91 V	nd	12	nd	38
g	[**Ni-2**]$^{2+}$	CyI	3	−1.91 V	nd	24	nd	nd

Figure 3. Controlled-potential electrolysis (CPE) reactivity data for **11** conducted in a divided electrochemical cell (0.044 mmol **11**, 0.004 mmol catalyst, 0.097 mmol additive in 5 mL catholyte). Charged passed until background current values observed and reported with respect to the amount of **11** added. In all cases, > 99% conversion of **11** observed. ^{1}H NMR yields against 1-methyloxindole standard reported due to low concentration of substrates utilized to match electroanalytical conditions. *Isolated yields also reported. For entry c, CPE was first conducted on [**Ni-1**]$^{2+}$ alone at 2 C mol^{-1} to form electrogenerated [**Ni-1**] (e-[**Ni-1**]), after which the applied potential bias was removed and **11** was added; product distribution investigated after stirring at RT for approximately 5 hours.

defined CV responses in the presence of **3** and/or CyI. These aromatic redox mediators exhibited responses consistent with known limiting cases of two kinetic regimes (total catalysis or catalyst deactivation),[54,64] allowing for the estimation of k_1 in the absence of convoluting side reactions (see **Figures S10-S17** and SI for experimental and theoretical details). In short, these methods provided consistent values of k_1 across varying experimental conditions, supporting the proposed mechanism involving rate-limiting activation of RI by the examined Ar redox mediators. The k_1 values found using this procedure are listed in **Table S3** and graphically represented in **Figure 2c**. The values found for CyI agree with reported k_1 values for the secondary alkyl iodide, 2-iodobutane,[55] providing further support for the methods utilized herein. As anticipated for OSET processes in which the transfer coefficients do not significantly change with the driving force,[53,59–61] an approximate log-linear relationship between the $E_{1/2}$ and k_1 is observed for RI activation by **4**-**10**, **Figure 2c**. Importantly, we find that the measured k_1 values for both **3** and CyI activation by [**Ni-1**] follows this approximate linear trend, providing strong evidence for OSET activation of **3** and CyI by [**Ni-1**]. While we note the logk_1-$E_{1/2}$ relationships, in theory, are nonlinear,[27,55,62] the slopes for the obtained linear fits, **Figure 2** (for **3**, –6.6±0.3, red and for CyI, –7.0±0.1, blue), allow us to estimate a transfer coefficient value of 0.4, consistent with previous reports detailing homogeneous concerted dissociative electron transfers to similar alkyl halide substrates[27,55,62] by Ar redox mediators. The consistently observed ~3-fold difference in rate between **3** and CyI suggests that the RI bond of **3** is indeed more activated than that of CyI, and thus more readily cleaved. The observed approximate log-linear relationship of k_1 with $E_{1/2}$ for RI activation by [**Ni-1**] with various electrogenerated Ar•$^-$ further supports the hypothesized mechanistic sequence invoked in steps 1-4 (*vide supra*) over an SN2-type activation by [**Ni-1**] to directly form [(**Ni-1**)(R)]; the latter inner-sphere reaction sequence would lead to higher rates that would significantly deviate from the values obtained for Ar•$^-$, e.g. as has been observed for alkyl bromide activation by iron porphyrin systems.[62] Together, these studies are consistent with a mechanism implicating dissociative OSET activation of RI by [**Ni-1**].

To decipher the downstream reactivity of the hypothesized [(**Ni-1**)(R)] species, *i.e.* step 4 in the proposed sequence, and the presence of free radical intermediates upon dissociative cleavage of RI, we examined the bulk electrolysis product distribution of [**Ni-1**]-catalyzed cyclization of **11**. As the cyclization of 5-hexenyl radical is expected to be fast and irreversible,[65] we reasoned that interrogation of the bulk electrolysis reactivity of **3** modified with an alkene would facilitate detection of cyclized products, indicative of free radical intermediates. First, to obtain the baseline reactivity of **11** in the absence of [**Ni-1**]$^{2+}$, controlled-potential electrolysis (CPE) of **11** was conducted at –2.73 V, corresponding to the potential associated with direct reduction (**Figure S8a**). This process gives rise to **12** following the passage of 2 C mol^{-1} of charge, **Figure 3**, entry a. These data are consistent with the reported[66] and observed, **Figure S8a**, two-electron CV waves associated with reduction of primary alkyl iodides, implicating that the reduction of **11** proceeds via the intermediacy of an electrogenerated carbanion. The observed 1,2 ester shift[67,68] of **12** further supports the presence of the carbanion intermediate. This reactivity lies in contrast to the high chemical yields observed for radical capture by alkenes for carbon-centered radicals electrogenerated from secondary halides,[19] highlighting the utility of redox mediation for primary alkyl halide substrates to synthetize cyclized products, *vide infra*, when direct reduction selectively forms the protodehalogenated product.[69] We note the low chemical yields observed (<100% carbon balance) for the CPE experiments, shown in **Figure 3**, which can be explained by the known functionalization of carbon surfaces under similar electrochemical conditions[63] and may be further exacerbated by the activated RI substrate utilized in this work.

CPE performed in the presence of catalytic amounts of [**Ni-1**]$^{2+}$ show product distributions consistent with the formation of radical intermediates produced via SET. In the presence of 10 mol % [**Ni-1**]$^{2+}$, CPE of **11** at –2.03 V, corresponding to the potential associated with mediated reduction (**Figure 2a**) gives rise to 31% and 17% yield of cyclized products **13** and **14**, respectively, following the passage of 1 C mol^{-1} of charge with respect to **11** (**Figure 3**, entry b). The observed electron stoichiometry is in line with the 1 C mol^{-1} value expected for the proposed bimolecular activation of **3**, *vide supra*. For **13**, we propose that the cyclized radical is quenched by an H-atom donor present in solution, which we hypothesize is DMF.[28,70] For **14**, the cyclized radical is quenched by a halogen atom donor; we

postulate that an equivalent of unreacted **11** could serve as the donor via an atom transfer radical (ATR) cyclization pathway.[12,71,72] To rule out the predominance of a non-Faradaic ATR chain pathway on the observed reactivity for **14**, we investigated the reactivity of **11** in the presence of electrogenerated [**Ni-1**] in the absence of potential bias. [**Ni-1**] was electrogenerated in the absence of **11** until 2 C mol^{-1} of charge with respect to $[\mathbf{Ni\text{-}1}]^{2+}$ was consumed, after which **4** was added and the potential was turned off. Products were not detected in quantifiable amounts (**Figure 3**, entry c) indicating that non-Faradaic chain processes do not predominate the observed reactivity. We repeated these experiments in the presence of triflate anions (OTf^-), which we observed redirects the product selectivity through a hypothesized coordination blocking mode. The presence of OTf^- dramatically changes the product distribution, with the dimer, **15**, being observed as the primary detectable product (**Figure 3**, entry d). These data suggest that OTf^- interacts with electrogenerated [**Ni-1**],[73] suppressing formation of the hypothesized [(**Ni-1**)(R)] species thereby favoring dimerization of free radicals formed via steps 1-3. Thus, we postulate that the observed reactivity in **Figure 3**, entry b, is due to the propensity of [(**Ni-1**)(R)] to act as a reductant towards another equivalent of **11**, thereby controlling the free radical behavior via the bimolecular oxidative addition pathway in steps 1-4. Together, these reactivity studies evince the formation of [**Ni-1**]-mediated free radical species and suggest the presence of a [(**Ni-1**)(R)] intermediate in directing the product selectivity.

Increased selectivity of radical processes is observed for [**Ni-1**]-catalyzed **11** activation performed in the presence of a viable halogen donor, CyI. Results show that 75% of **14** formed and 19% of **13** are formed (**Figure 3**, entry e). Importantly, only 1 C mol^{-1} charge is transferred, **Figure S18a**, indicative of selective activation of **11** over CyI and consistent with the discrimination in k_1 observed between the two substrates given in **Figure 2c**. The observation of high selectivity for **14** after the passage of 1 C mol^{-1} rules out the predominance of an ATR cyclization chain pathway,[12,71,72] which would lead to a significantly diminished and fractional electron equivalency as previously observed.[28] Thus, CyI serves as a halogen atom donor to quench the radical cascade sequence. Together, these data demonstrate that [**Ni-1**] catalyzes a selective radical process in an electrochemical environment: [**Ni-1**] selectively activates **11** over CyI in an OSET-initiated bimolecular event, the subsequent hypothesized [(**Ni-1**)(R)] further activates another equivalent of **11**, regenerating $[\mathbf{Ni\text{-}1}]^+$ and generating cyclized radicals that are quenched by CyI.

Single-Electron Activation of Alkyl Iodide Substrates by $[\mathbf{Ni\text{-}2}]^+$. In contrast to results obtained with $[\mathbf{Ni\text{-}1}]^{2+}$, corresponding electroanalytical data collected for $[\mathbf{Ni\text{-}2}]^{2+}$ implicate inner-sphere electron transfer (ISET) activation of the substrates examined, **3** and CyI. **Figure 2b** shows the CV of 0.9 mM $[\mathbf{Ni\text{-}2}]^{2+}$ in the absence (black dotted trace) and presence of 10 mM of **3** (red dotted trace). Upon the addition of **3**, the wave corresponding to $[\mathbf{Ni\text{-}2}]^{2+}/[\mathbf{Ni\text{-}2}]^+$ becomes irreversible and a j_P/j_0 value equalling 8 is observed. This value increases monotonically with added concentration of **3**, **Figure S19**, suggesting that, unlike [**Ni-1**], activation of **3** by $[\mathbf{Ni\text{-}2}]^+$ involves the continuous catalytic regeneration of $[\mathbf{Ni\text{-}2}]^{2+}$ at an appreciable rate. Similar results are obtained for data collected using CyI as the substrate. **Figure 2b** shows the CV of 1 mM $[\mathbf{Ni\text{-}1}]^{2+}$ in the absence (black dotted trace) and presence of 11 mM of CyI (blue dotted trace). When CyI is added, a j_P/j_0 value equalling 16 is observed at the peak corresponding to $[\mathbf{Ni\text{-}2}]^+$ formation. This value also increases monotonically with added concentration of CyI (**Figure S20).** A mechanistic sequence consistent with these observations is:

$$[\mathbf{Ni\text{-}2}]^{2+} + e^- \overset{k_s}{\rightleftharpoons} [\mathbf{Ni\text{-}2}]^+ \quad (5)$$

$$[\mathbf{Ni\text{-}2}]^+ + RI \overset{k_1}{\rightarrow} R\bullet + I^- + [\mathbf{Ni\text{-}2}]^{2+} \quad (6)$$

where k_s is the heterogeneous electron transfer rate obtained in the absence of substrate, *vide supra*. This mechanism is in line with a redox catalysis scheme,[64,74] where the homogeneous electron transfer step between electrogenerated catalyst (here, $[\mathbf{Ni\text{-}2}]^+$) and RI is rate-determining.[27] Within this mechanistic framework, a lower limit on k_1 can be estimated by constructing working curves, which depict theoretical j_P/j_0 values at varying $C_{RI}/C_{[\mathbf{Ni\text{-}2}]^{2+}}$ (see SI and **Figures S19**, **S20** for details). Agreement of the values across various substrate concentrations and scan rates were observed; average values of log k_1 = 5.7±0.2 [M^{-1} s^{-1}] and log k_1 = 7.1±0.2 [M^{-1} s^{-1}] (**Table S3** and **Figure 2c**, labeled red circle and blue square) were obtained for **3** and CyI, respectively. Comparison of these rates with those obtained for [**Ni-1**], **Figure 2c**, reveal that; (1) the k_1 values do not scale with those observed for Ar and [**Ni-1**]-mediated RI activation; and (2) $[\mathbf{Ni\text{-}2}]^+$ exhibits roughly 10-fold and 100-fold higher rates of activation for **3** and CyI, respectively, as $Ar\bullet^-$ and [**Ni-1**] with similar $E_{1/2}$. These data delineate that, unlike [**Ni-1**], RI activation by $[\mathbf{Ni\text{-}2}]^+$ is inconsistent with an OSET mechanism to regenerate an oxidized Ni species, $[\mathbf{Ni\text{-}2}]^{2+}$. These data suggest that, instead, ISET-based activation prevails for $[\mathbf{Ni\text{-}2}]^+$-catalyzed RI activation, resulting in a $[(\mathbf{Ni\text{-}2})(I)]^+$ intermediate in which the halogen atom is abstracted, i.e.

$$[\mathbf{Ni\text{-}2}]^+ + RI \overset{k_1}{\rightarrow} R\bullet + [(\mathbf{Ni\text{-}2})(I)]^+ \quad (7)$$

The existence of the proposed $[(\mathbf{Ni\text{-}2})(I)]^+$ intermediate is supported by the observation that independently synthesized and characterized $[Ni(PY5Me2)(I)]^+$ (see SI, **Table S4**, and **Figure S21**) exhibits similar electrochemical features to $[\mathbf{Ni\text{-}2}]^{2+}$. A single redox feature ($E_{1/2}$ = –1.75 V) is observed, which falls within the potential range in which catalysis is detected for $[\mathbf{Ni\text{-}2}]^{2+}$. Second, $[Ni(PY5Me2)(I)]^+$ exhibits a significant catalytic current response in the presence of **3**, consistent with the notion that catalysis can be initiated by entering the cycle from this intermediate. While the detailed structure of the substrate-$[\mathbf{Ni\text{-}2}]^+$ association complex that may enable an inner-sphere interaction cannot be determined from these data, it is clear that $[\mathbf{Ni\text{-}2}]^+$ does not activate RI via OSET.

To probe the downstream reactivity of hypothesized free radical intermediates generated in step 6, CPE experiments of **11** were performed in the presence of catalytic amounts of $[\mathbf{Ni\text{-}2}]^{2+}$. In the presence of 10 mol % of $[\mathbf{Ni\text{-}2}]^{2+}$, CPE of **11** at – 1.91 V, corresponding to the potential associated with mediated reduction, **Figure 2a**, gives rise to 12% and 38% yield of cyclized products **13** and **15**, respectively, following the passage of 1 C mol^{-1} of charge with respect to **11**, **Figure 3**, entry f. These data suggest that the observed higher rates of radical formation for $[\mathbf{Ni\text{-}2}]^+$ vs [**Ni-1**]-catalyzed RI activation, **Figure 2c**, leads to a higher concentration that favors dimerization. To verify that dimerized products are not a result of metal-mediated reductive elimination, we performed CPE of **11** in the presence of 10 mol% of Ar, **8**, and obtained exclusive formation of **15**, suggesting that dimerization is favored due to the high rates of sub-

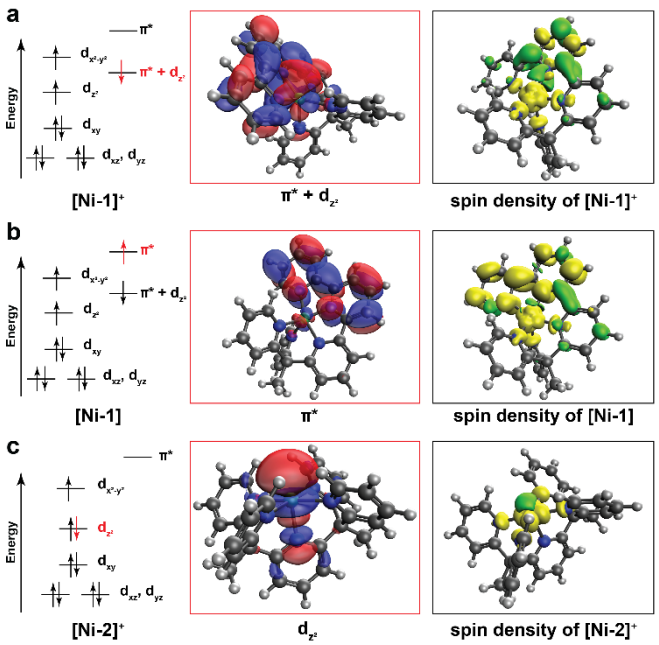

Figure 4. DFT analysis of electrochemically accessible reduced species, [**Ni-1**]$^{+}$ (**a**), [**Ni-1**] (**b**), and [**Ni-2**]$^{+}$ (**c**). For each species the following are shown: (1) simplified, qualitative molecular orbital diagram (**left**) consistent with DFT calculations, where newly added electron (relative to unreduced state) is highlighted in red; (2) relevant calculated MO (**middle red box**); and (3) the calculated spin density plot (**right black box**). Molecular orbitals not to scale.

strate activation. The existence of the proposed [(**Ni-2**)(I)]$^{+}$ intermediate, Equation 6, is further supported by the observation that CPE of **11** in the presence of 10 mol% of independently synthesized [Ni(PY5Me2)(I)]$^{+}$ exhibits a similar product distribution, favoring formation of **15**, under electrocatalytic conditions after the passage of 1 C mol^{-1}, **Figure S21**. In addition, [Ni(PY5Me2)(I)]$^{+}$ exhibits a redox feature ($E_{1/2}$ = –1.75 V) more positive than the potential utilized for CPE experiments in **Figure 3** (–1.91 V), demonstrating that reduced Ni species from the proposed [Ni(PY5Me2)(I)]$^{+}$ can be accessed within the potential value utilized for CPE. This result demonstrates that the proposed [(**Ni-2**)(I)]$^{+}$ intermediate is catalytically viable, and further supports the proposed ISET mechanism. Finally, in contrast to the reactivity observed for [**Ni-1**], increased selectivity for radical products are not observed when the reaction is conducted in the presence of CyI (**Figure 3**, entry g). Instead, indiscriminate activation of CyI and **11** are observed as evidenced by the 3 C mol^{-1} charge consumption, **Figure S18b**, and ensuing complex distribution of products, where only a small amount of **13** could be identified. These data are consistent with the high k_1 observed for both substrates in **Figure 2c**, and thus simultaneous activation of both **11** and CyI are observed, resulting in unselective radical processes. Together, these data evince the formation of free radical intermediate species and demonstrate that [**Ni-2**]$^{+}$ catalyzes SET reductive activation of RI at higher rates than [**Ni-1**] owning to an inner-sphere interaction, manifesting in higher selectivity for the formation of unproductive dimerized products and indiscriminate activation of **11** and CyI.

Computational Characterization of Reduced Electroactive Species [Ni-1] and [Ni-2]$^{+}$. Computational analysis provide insight into the molecular orbital composition and occupancies of the electroactive Ni species responsible for SET activation of RI. **Tables S5-S7** show the coordinates for optimized structures for [**Ni-1**]$^{2+}$, [**Ni-1**]$^{+}$, and [**Ni-1**] obtained using DFT calculations employing ωB97X-D functionals and DMF as the solvent. The computed redox potentials (E^0 = –1.27 V and –2.06 V), and the spin state (S = 1) for [**Ni-1**]$^{2+}$ are consistent with experimentally determined values (**Figures S22a** and **b**). DFT calculations predict that the first reduction of [**Ni-1**]$^{2+}$ to [**Ni-1**]$^{+}$ is accompanied by the loss of the axial solvent molecule and the population of a low-lying mixed metal-ligand (π^* + d_{z2}, 35% Ni-d) orbital, resulting in a doublet ground state (S = 1/2), **Figure 4a**, left and middle. The spin density plot for [**Ni-1**]$^{+}$ (**Figure 4a** right) suggests that the excess spin is delocalized between the ligand and the metal. This molecular description of reduced tpy ligand over a purely metal-based reduction is in agreement with: (1) EPR and computational studies of [Ni(tpy)(CH$_3$)]$^{+}$, which describe the complex as (Ni(II)-CH$_3$)$^{+}$ bound to a one-electron-reduced π radical monoanion (tpy•)$^{-}$;[75] (2) computational studies on the structurally analogous [Fe(tpyPY2Me)(MeCN)]$^{+}$,[45] which describe the complex as Fe(II) bound to (tpyPY2Me•)$^{-}$; and (3) spectroscopic and computational studies,[76] describing reduced [Cr(tpy)$_2$]$^{2+}$ as Cr(III) bound to (tpy•)$^{-}$ in addition to the neutral parent ligand, (tpy^0). DFT calculations predict that the second reduction of [**Ni-1**]$^{+}$ to [**Ni-1**] is associated with the population of a primarily ligand-based orbital (π^*) to form a triplet ground state (S = 1), **Figure 4b,** left and middle. This second reduction is also accompanied by a rearrangement of the π^* + d_{z2} orbital, occupied by the first excess electron, to form a more metal-based orbital (π^* + d_{z2}, 48% Ni-d), **Figure S23**. The spin density plots for [**Ni-1**] reveal that the excess spin is delocalized between the ligand and the metal, **Figure 4b**, right. Thus, the computational data suggest that electroactive [**Ni-1**] species can be described by a resonance form of the following: (1) a reduced Ni(I) center bound to (tpyPY2Me•)$^{-}$; and (2) an unreduced Ni(II) center bound to (tpyPY2Me••)$^{2-}$. Together, these data suggest that the two observed redox events for [**Ni-1**]$^{2+}$ occur in a delocalized fashion onto both the Ni center and the tpyPY2Me ligand, and that this spin delocalized [**Ni-1**] complex is responsible for the observed RI activation reactivity.

In contrast, DFT analyses for [**Ni-2**]$^{2+}$ are consistent with a purely metal-based reduction event. **Tables S8** and **S9** show the coordinates obtained for optimized structures of [**Ni-2**]$^{2+}$ and [**Ni-2**]$^{+}$, respectively. The computed redox potential (E^0 = –1.77 V), and the spin state (S = 1) for [**Ni-2**]$^{2+}$ are in line with experimentally determined values (**Figures S21c** and **d**). DFT calculations predict that the reduction of [**Ni-2**]$^{2+}$ to [**Ni-2**]$^{+}$ is accompanied by the loss of the axial solvent molecule and the population of a purely metal-based (d_{z2}) orbital, resulting in a doublet ground state (S = 1/2) (**Figure 4c**, left and middle) and the formation of a Ni(I) species. The spin density plot for [**Ni-1**]$^{+}$ given in **Figure 4c** (right) similarly suggests that the excess spin is localized on the metal. Metal-localized reduction and concomitant nuclear reconfiguration offer a possible explanation for the sluggishness of the electron transfer rate (k_s) observed by CV studies, *vide supra*.[77] Together, these data establish that unlike [**Ni-1**]$^{2+}$, [**Ni-2**]$^{2+}$ reduction proceeds solely at the Ni center, strongly implicating that a metal localized [**Ni-1**]$^{+}$ system is responsible for the observed RI activation reactivity.

Mechanistic Model for Controlled Single Electron Transfer Manipulated via Metal-Ligand Cooperativity. The combined insights from electroanalytical, electrosynthetic, and computational studies point to a model where the extent of the Ni metal-centered reduction alters the mechanism for SET activation of RI substrates. For electrogenerated [**Ni-1**], **Figure 5**,

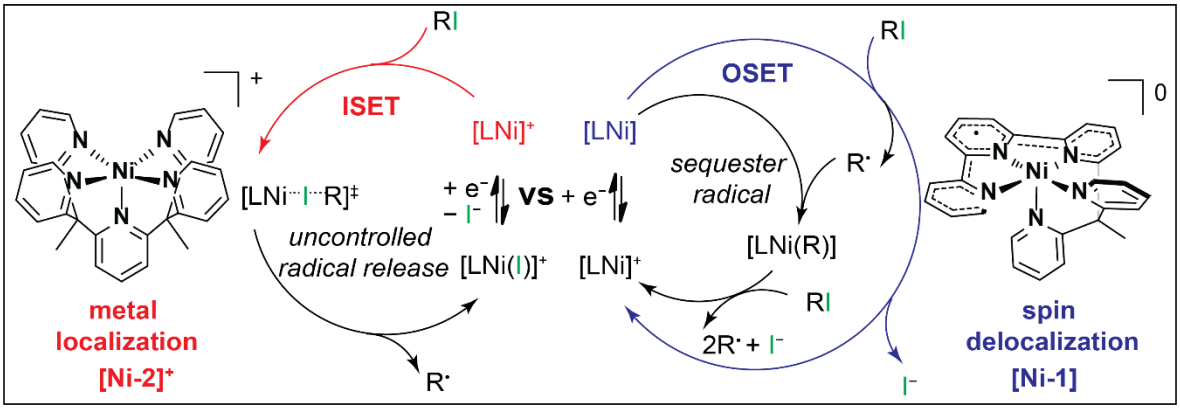

Figure 5. Mechanistic model for alkyl radical generation by [Ni(PY5Me2)]$^+$ (**left**) and [Ni(tpyPY2Me)] (**right**).

right, computational results describe the electroactive reduced complex as one where the excess spin is delocalized throughout the π system, **Figure 4b**. Electroanalytical data are consistent with a purely OSET activation manifold of investigated model substrates **3** and CyI by the spin delocalized [**Ni-1**], where rate-limiting RI bond cleavage rates scale with those obtained for metal-free redox mediators, **Figure 2c**. Electroanalytical data are also in line with an electron stoichiometry whereby the ensuing alkyl radical rapidly recombines with another equivalent of [**Ni-1**] to enable an overall bimolecular oxidative addition pathway (**Figures 2a**, **2b**, **S6**, **S7**, and **S9**). While obtaining definitive structural evidence for the postulated in-situ formed [LNi(R)] has remained challenging due to its reactive nature, the present data rule out the alternative mechanism of an OSET pathway that does not involve alkyl rebound. This alternative mechanism would result in an electrocatalytic wave that monotonically increases as a function of the substrate concentration. Instead, we demonstrate that the presence of RI substrates leads to a two-fold current enhancement that does not increase with further addition of RI. In addition, if such a pathway were operative, product distributions following CPE conducted under catalytic conditions would remain unaffected by changes in the counteranion. However, we observe that the presence of OTf$^-$ induces the formation of unproductive dimerization of cyclized products from substrate **11** whereas its absence disfavors dimerization. Thus, these studies are consistent with the hypothesis that free radical species (R•) are formed that interact with [**Ni-1**] under electrocatalytic conditions.

These insights enable us to build the mechanistic model shown in **Figure 5**, right. The OSET mechanism contrasts with related RI activation processes catalyzed by [Ni(tpy)(CH$_3$)]$^+$; it has been hypothesized[78] and computed[79] to proceed via rate-limiting halogen atom transfer followed by radical formation and rebound. We propose that the OSET pathway found here is favored due to the spin delocalization in both [**Ni-1**] and [**Ni-1**]$^+$ imparted by the redox-active, rigid, pentadentate tpyPY2Me scaffold because: (1) spin delocalization imparts reduced interaction with σ* of the RI substrates; and (2) the tpyPY2Me serves to stabilize these redox states as evidenced by their Nernstian CV behavior. We postulate that the OSET mechanism allows for the discrimination in k_1 observed for CyI vs **3**, giving rise to selective activation of **11** in the presence of the halogen atom donor, CyI. We hypothesize that the [LNi(R)] species can either: (1) reduce another equivalent of RI; and/or (2) release products by protodemetallation. The former mechanism is consistent with the observation of 1 C mol^{-1} of RI charge consumption, and therefore, we depict this model in **Figure 5**. Thus, this mechanistic model proposes that RI activation via [**Ni-1**] enables the controlled electrogeneration and sequestration of R•, facilitating selective free radical reactivity in an electrochemical environment.

Our combined data are consistent with a contrasting mechanistic pathway for RI activation by [**Ni-2**]$^+$ bearing the redox-inactive PY5Me2 ligand. For electrogenerated [**Ni-2**]$^+$, **Figure 5**, left, computational studies are in line with the expected purely metal-localized reduction, **Figure 4c**. Electroanalytical data are inconsistent with an OSET manifold for activating **3** and CyI, **Figure 2c**. Thus, we postulate that an electrocatalytic ISET activation pathway is favored due to an enhanced interaction of the σ* of the RI substrates with the localized reduced metal center, leading to a formal halogen atom abstraction past the rate-limiting RI bond cleavage step to form[(**Ni-2**)(I)]$^+$. As such, [**Ni-2**]$^+$ activates both CyI and **3** at much higher rates than [**Ni-1**] at comparable applied potentials, precluding the selective activation of one substrate over another, **Figure 2c** and **Figure 3**. In addition, this mechanistic postulate explains the discrimination in k_1 observed for **3** vs. CyI activation by [**Ni-2**]$^+$, **Figure 2c**, the more sterically encumbered substrate **3** exhibits lower rates than CyI within experimental error. Electrosynthetic studies are consistent with the high rate of formation for free radical species following electrocatalytic RI activation; higher selectivity for unproductive dimerization of cyclized products are obtained from **11**, **Figure 3**, in comparison to that obtained using [**Ni-1**]. Finally, we provide additional support for the proposed [(**Ni-2**)(I)]$^+$ intermediate by demonstrating that catalysis can be initiated by entering the cycle from this species. We independently synthesized the compound and revealed that it exhibited electrocatalytic features in the presence of the substrate and high selectivity towards unproductive dimerization, similar to what we observe for catalysis by [**Ni-2**]$^+$. **Figure 5**, left, summarizes the proposed mechanism of RI activation by [**Ni-2**]$^+$.

Comparison of this proposal with the mechanistic model for [**Ni-1**]-mediated RI activation, **Figure 5** demonstrates that the rate of electrocatalytic radical generation, and thus selectivity of downstream radical products, can be controlled via ligand-directed manipulation of the single electron transfer mechanism. As increased rates of SET RI activation would result in increased concentration of R•, the model shows that ISET activation by [**Ni-2**]$^+$ generates a high R• concentration for both **3** and CyI while [**Ni-1**] allows for controlled radical generation dictated by the potential difference of $E_{1/2}$ of [**Ni-1**]$^+$ and the standard potential for RI reduction. Taken together, these mechanistic studies highlight how tuning the extent of metal-centered reduction via metal-ligand cooperativity directs OSET vs ISET

pathways for electrocatalyzed alkyl halide activation, thereby establishing a generalizable molecular design principle for the development of selective free radical-based catalytic sequences in an electrochemical environment.

CONCLUSION

In this work, we report the synthesis, electrochemical characterization, reactivity for single electron transfer activation of alkyl iodides, and electronic structure calculations of Ni complexes that differ in the ligand manifold by the presence and absence of a redox-active terpyridine moiety. We combine electroanalytical studies and bulk electrolysis reactivity data to formulate the mechanistic basis for the divergent selectivity toward redox-mediated radical reactivity we observe for the two complexes. We identify that Ni-ligand cooperativity enables control over the single electron transfer substrate activation pathway, limiting undesired radical recombination products and promoting a selective model radical process. These studies reveal that tuning the extent of metal-centered reduction can be used to control the electron transfer mechanism, and thereby, radical-based electroorganic reaction selectivity.

At a fundamental level, our studies establish distinct rate and potential requirements for redox mediator design compared to those typically pursued in formulating molecular electrocatalyst design principles. For applications in energy conversion catalysis, for example, molecular electrocatalysts with the highest turnover frequencies at the lowest applied potentials are targeted; as they enable the most efficient fuel-formation.[80] In contrast, we find that in order to achieve selective free radical reactivity in an electrochemical environment, molecular electrocatalysts operative at the highest rates at low potentials, in this case [**Ni-2**]$^{+}$, are *not* the ideal catalysts as unproductive dimerization outcompetes the desired reactivity and indiscriminate activation of various substrates is observed. Instead, we demonstrate that catalysts with *fine-tuned* and lower rates of activation at low potentials, [**Ni-1**], exhibit higher selectivities for cyclized products. These results highlight how fine-tuned rates may be more applicable criteria to target when developing new catalysts for electroorganic applications involving free radical intermediates. Furthermore, while we note that these findings cannot be extrapolated to electrocatalytic systems beyond Ni-catalyzed alkyl iodide activation at this time, our findings lie in contrast to the contemporary view that the electron distribution plays a minor role for reactions proceeding via outer sphere electron transfer and a major role for those proceeding via inner-sphere pathways.[81] For reactions where all-organic redox mediators are readily deactivated, as is the case for mediated primary alkyl radical generation, we show that metal-ligand cooperativity *enables* sustained outers-sphere electron transfer to proceed in cases where inner-sphere pathways yields substrate activation rates that are intractable for selective radical reactions. Together, this work serves to demonstrate how electrocatalyst ligand design coupled with electroanalysis serve as powerful tools towards establishing molecular level insights that underpin electroorganic reaction selectivity in complex electrochemical environments.

ASSOCIATED CONTENT

Supporting Information. Experimental and computational details and methods are listed in the SI. Synthetic procedures, electrochemical data, simulations, spectroscopic data, quantum chemical calculations, and x-ray crystallographic data. CIF files for crystal structures. This material is available free of charge via the Internet at http://pubs.acs.org.

AUTHOR INFORMATION

Corresponding Author

*fdtoste@berkeley.edu
*chrischang@berkeley.edu

ACKNOWLEDGMENT

This research was supported by the Director, Office of Science, Office of Basic Energy Sciences, and the Division of Chemical Sciences, Geosciences, and Bioscience of the U.S. Department of Energy at Lawrence Berkeley National Laboratory (Grant No. DE-AC02-05CH11231 to F.D.T. and C.J.C.), a post-doctoral fellowship to A. W. (NRSA 5F32GM130025), and a graduate fellowship to J.S.D. (Chevron). We thank Dr. Miao Zhang for assistance with MS data collection, Prof. Cyrille Constentin for discussions on electrochemical analysis, Dr. Spencer Scholz for discussions on relevant literature and detailed reading of the manuscript, and the Joint Center for Energy Storage Research (JCESR) for the electrochemical cell.

REFERENCES

(1) Chatgilialoglu, C.; Ferreri, C.; Landais, Y.; Timokhin, V. I. Thirty Years of (TMS)3SiH: A Milestone in Radical-Based Synthetic Chemistry. *Chem. Rev.* **2018**, *118* (14), 6516–6572.

(2) Neumann, W. P. Tri-n-Butyltin Hydride as Reagent in Organic Synthesis. *Synthesis (Germany)*. Georg Thieme Verlag September 12, 1987, pp 665–683.

(3) Yorimitsu, H.; Oshima, K. Radical Chain Reactions: Organoborane Initiators. In *Radicals in Organic Synthesis*; Wiley-VCH Verlag GmbH: Weinheim, Germany, 2008; pp 11–27.

(4) Renaud, P.; Sibi, M. P. *Radicals in Organic Synthesis*; Wiley-VCH: Weinheim, 2001.

(5) Constantin, T.; Zanini, M.; Regni, A.; Sheikh, N. S.; Juliá, F.; Leonori, D. Aminoalkyl Radicals as Halogen-Atom Transfer Agents for Activation of Alkyl and Aryl Halides. *Science* **2020**, *367* (6481), 1021–1026.

(6) Kuo, J. L.; Lorenc, C.; Abuyuan, J. M.; Norton, J. R. Catalysis of Radical Cyclizations from Alkyl Iodides under H2: Evidence for Electron Transfer from [CpV(CO)3H]-. *J. Am. Chem. Soc.* **2018**, *140* (13), 4512–4516.

(7) Kim, H.; Lee, C. Nickel-Catalyzed Reductive Cyclization of Organohalides. *Org. Lett.* **2011**, *13* (8), 2050–2053.

(8) Kim, H.; Lee, C. Visible-Light-Induced Photocatalytic Reductive Transformations of Organohalides. *Angew. Chem. Int. Ed.* **2012**, *51* (49), 12303–12306.

(9) Nguyen, J. D.; D'Amato, E. M.; Narayanam, J. M. R.; Stephenson, C. R. J. Engaging Unactivated Alkyl, Alkenyl and Aryl Iodides in Visible-Light-Mediated Free Radical Reactions. *Nat. Chem.* **2012**, *4* (10), 854–859.

(10) Shen, Y.; Cornella, J.; Juliá-Hernández, F.; Martin, R. Visible-Light-Promoted Atom Transfer Radical Cyclization of Unactivated Alkyl Iodides. *ACS Catal.* **2017**, *7* (1), 409–412.

(11) Alpers, D.; Gallhof, M.; Witt, J.; Hoffmann, F.; Brasholz, M. A Photoredox-Induced Stereoselective Dearomative Radical (4+2)-Cyclization/1,4-Addition Cascade for the Synthesis of Highly Functionalized Hexahydro-1 H -Carbazoles. *Angew. Chem. Int. Ed.* **2017**, *56* (5), 1402–1406.

(12) Gu, X.; Li, X.; Qu, Y.; Yang, Q.; Li, P.; Yao, Y. Intermolecular Visible-Light Photoredox Atom-Transfer Radical [3+2]-Cyclization of 2-(Iodomethyl)Cyclopropane-1,1-Dicarboxylate with Alkenes and Alkynes. *Chem. - A Eur. J.* **2013**, *19* (36), 11878–11882.

(13) Murphy, J. A.; Khan, T. A.; Zhou, S. Z.; Thomson, D. W.; Mahesh, M. Highly Efficient Reduction of Unactivated Aryl and Alkyl Iodides by a Ground-State Neutral Organic Electron Donor. *Angew. Chem. Int. Ed.* **2005**, *44* (9), 1356–1360.

(14) Hwang, J. Y.; Baek, J. H.; Shin, T. Il; Shin, J. H.; Oh, J. W.; Kim,

K. P.; You, Y.; Kang, E. J. Single-Electron-Transfer Strategy for Reductive Radical Cyclization: Fe(CO)5 and Phenanthroline System. *Org. Lett.* **2016**, *18* (19), 4900–4903.
(15) Li, D.; Ma, T. K.; Scott, R. J.; Wilden, J. D. Electrochemical Radical Reactions of Alkyl Iodides: A Highly Efficient, Clean, Green Alternative to Tin Reagents. *Chem. Sci.* **2020**, *11* (20), 5333–5338.
(16) Crespi, S.; Fagnoni, M. Generation of Alkyl Radicals: From the Tyranny of Tin to the Photon Democracy. *Chem. Rev.* **2020**, *120* (17), 9790–9833.
(17) Sebren, L. J.; Devery, J. J.; Stephenson, C. R. J. Catalytic Radical Domino Reactions in Organic Synthesis. *ACS Catalysis*. 2014, pp 703–716.
(18) Bohn, M. A.; Paul, A.; Hilt, G. Electrochemically Initiated Radical Reactions. *Encyclopedia of Radicals in Chemistry, Biology and Materials*; John Wiley & Sons, Ltd, 2012; pp 1–40.
(19) Zhang, W.; Lin, S. Electroreductive Carbofunctionalization of Alkenes with Alkyl Bromides via a Radical-Polar Crossover Mechanism. *J. Am. Chem. Soc.* **2020**, *142* (49), 20661–20670.
(20) Narayanam, J. M. R.; Tucker, J. W.; Stephenson, C. R. J. Electron-Transfer Photoredox Catalysis: Development of a Tin-Free Reductive Dehalogenation Reaction. *J. Am. Chem. Soc.* **2009**, *131* (25), 8756–8757.
(21) Tucker, J. W.; Narayanam, J. M. R.; Krabbe, S. W.; Stephenson, C. R. J. Electron Transfer Photoredox Catalysis: Intramolecular Radical Addition to Indoles and Pyrroles. *Org. Lett.* **2010**, *12* (2), 368–371.
(22) Juris, A.; Balzani, V.; Barigelletti, F.; Campagna, S.; Belser, P.; von Zelewsky, A. Ru(II) Polypyridine Complexes: Photophysics, Photochemistry, Eletrochemistry, and Chemiluminescence. *Coord. Chem. Rev.* **1988**, *84* (C), 85–277.
(23) Connell, T. U.; Fraser, C. L.; Czyz, M. L.; Smith, Z. M.; Hayne, D. J.; Doeven, E. H.; Agugiaro, J.; Wilson, D. J. D.; Adcock, J. L.; Scully, A. D.; et al. The Tandem Photoredox Catalysis Mechanism of [Ir(Ppy)2(Dtb-Bpy)]+ Enabling Access to Energy Demanding Organic Substrates. *J. Am. Chem. Soc.* **2019**, *141* (44), 17646–17658.
(24) Duñach, E.; José Medeiros, M.; Olivero, S. Intramolecular Reductive Cyclisations Using Electrochemistry: Development of Environmentally Friendly Synthetic Methodologies. *New J. Chem.* **2006**, *30* (11), 1534–1548.
(25) Duñach, E.; Medeiros, M. J.; Olivero, S. Electrochemical Cyclizations of Organic Halides Catalyzed by Electrogenerated Nickel(I) Complexes: Towards Environmentally Friendly Methodologies. *Electrochim. Acta* **2017**, *242*, 373–381.
(26) Francke, R.; Little, R. D. Redox Catalysis in Organic Electrosynthesis: Basic Principles and Recent Developments. *Chem. Soc. Rev.* **2014**, *43* (8), 2492–2521.
(27) Lexa, D.; Savéant, J. M.; Su, K. B.; Wang, D. L. Chemical vs. Redox Catalysis of Electrochemical Reactions. Reduction of Trans-1,2-Dibromocyclohexane by Electrogenerated Aromatic Anion Radicals and Low Oxidation State Metalloporphyrins. *J. Am. Chem. Soc.* **1987**, *109* (21), 6464–6470.
(28) Ozaki, S.; Matsushita, H.; Ohmori, H. Indirect Electroreductive Cyclisation of N-Allylic and N-Propargylbromo Amides and o-Bromoacryloylanilides Using Nickel(II) Complexes as Electron-Transfer Catalysts. *J. Chem. Soc. Perkin Trans. 1* **1993**, No. 19, 2339–2344.
(29) Foley, M. P.; Du, P.; Griffith, K. J.; Karty, J. A.; Mubarak, M. S.; Raghavachari, K.; Peters, D. G. Electrochemistry of Substituted Salen Complexes of Nickel(II): Nickel(I)-Catalyzed Reduction of Alkyl and Acetylenic Halides. *J. Electroanal. Chem.* **2010**, *647* (2), 194–203.
(30) Duñach, E.; Esteves, A. P.; Medeiros, M. J.; Olivero, S. Electrochemical Intramolecular Cyclisation of Propargyl Bromoethers Catalysed by Nickel Complexes. *New J. Chem.* **2005**, *29* (4), 633–636.
(31) Duñach, E.; Esteves, A. P.; Freitas, A. M.; Medeiros, M. J.; Olivero, S. Electroreductive Cyclisation of Unsaturated Halides Catalysed by Nickel Macrocyclic Complexes. *Tetrahedron Lett.* **1999**, *40* (49), 8693–8696.
(32) Diccianni, J. B.; Katigbak, J.; Hu, C.; Diao, T. Mechanistic Characterization of (Xantphos)Ni(I)-Mediated Alkyl Bromide Activation: Oxidative Addition, Electron Transfer, or Halogen-Atom Abstraction. *J. Am. Chem. Soc.* **2019**, *141* (4), 1788–1796.
(33) Ihara, M.; Katsumata, A.; Setsu, F.; Tokunaga, Y.; Fukumoto, K. Synthesis of Six-Membered Compounds by Environmentally Friendly Cyclization Using Indirect Electrolysis. *J. Org. Chem.* **1996**, *61* (2), 677–684.
(34) Esteves, A. P.; Neves, C. S.; Medeiros, M. J.; Pletcher, D. Organic Cyclisations of Propargyl and Allyl Bromoesters in Microemulsions Catalysed by Electrogenerated Nickel(I) Tetramethylcyclam. *J. Electroanal. Chem.* **2008**, *614* (1–2), 131–138.
(35) Duñach, E.; Esteves, A. P.; Freitas, A. M.; Lemos, M. A.; Medeiros, M. J.; Olivero, S. Intramolecular Cyclization of Propargyl Derivatives Using Environmentally Friendly Methodologies. *Pure Appl. Chem.* **2001**, *73* (12), 1941–1945.
(36) Duñach, E.; Esteves, A. P.; Medeiros, M. J.; Olivero, S. Electrogenerated Nickel(I) Complexes as Catalysts for the Intramolecular Radical Cyclisation of Unsaturated α-Bromoesters. *Tetrahedron Lett.* **2004**, *45* (42), 7935–7937.
(37) Gosden, C.; Healy, K. P.; Pletcher, D. Reaction of Electrogenerated Square-Planar Nickel(I) Complexes with Alkyl Halides. *J. Chem. Soc. Dalt. Trans.* **1978**, *4* (8), 972–976.
(38) Bakac, A.; Espenson, J. H. Kinetics and Mechanism of the Alkylnickel Formation in One-Electron Reductions of Alkyl Halides and Hydroperoxides by a Macrocyclic Nickel(I) Complex. *J. Am. Chem. Soc.* **1986**, *108* (4), 713–719.
(39) Becker, J. Y.; Kerr, J. B.; Pletcher, D.; Rosas, R. The Electrochemistry of Square Planar Macrocyclic Nickel Complexes and the Reaction of Ni(I) with Alkyl Bromides: Nickel Tetraamine Complexes. *J. Electroanal. Chem.* **1981**, *117* (1), 87–99.
(40) Esteves, A. P.; Freitas, A. M.; Medeiros, M. J.; Pletcher, D. Reductive Intramolecular Cyclisation of Unsaturated Halides by Ni(II) Complexes. *J. Electroanal. Chem.* **2001**, *499* (1), 95–102.
(41) Azevedo, F.; Freire, C.; De Castro, B. Reductive Electrochemical Study of Ni(II) Complexes with N2O2 Schiff Base Complexes and Spectroscopic Characterisation of the Reduced Species. Reactivity towards CO. *Polyhedron* **2002**, *21* (17), 1695–1705.
(42) Gosden, C.; Kerr, J. B.; Pletcher, D.; Rosas, R. The Electrochemistry of Square Planar Macrocyclic Nickel Complexes and the Reaction of Ni(I) with Alkyl Bromides: Tetradentate Schiff Base Complexes. *J. Electroanal. Chem.* **1981**, *117* (1), 101–107.
(43) Gosden, C.; Pletcher, D. The Catalysis of the Electrochemical Reduction of Alkyl Bromides by Nickel Complexes: The Formation of Carboncarbon Bonds. *J. Organomet. Chem.* **1980**, *186* (3), 401–409.
(44) Martin, E. T.; McGuire, C. M.; Peters, D. G. Catalytic Reduction of Organic Halides by Electrogenerated Nickel(I) Salen. *Electrochem. Soc. Interface* **2016**, *25* (2), 41–45.
(45) Derrick, J.; Loipersberger, M.; Iovan, D.; Smith, P. T.; Chakarawet, K.; Yano, J.; Long, J. R.; Head-Gordon, M.; Chang, C. Metal–Ligand Exchange Coupling Promotes Iron-Catalyzed Electrochemical CO2 Reduction at Low Overpotentials. *J. Am. Chem. Soc.* **2020**, *142* (48), 20489–20501.
(46) Hartmann, M.; Studer, A. Cyclizing Radical Carboiodination, Carbotelluration, and Carboaminoxylation of Aryl Amines. *Angew. Chem. Int. Ed.* **2014**, *53* (31), 8180–8183.
(47) Karunadasa, H. I.; Chang, C. J.; Long, J. R. A Molecular Molybdenum-Oxo Catalyst for Generating Hydrogen from Water. *Nature* **2010**, *464* (7293), 1329–1333.
(48) Bechlars, B.; D'Alessandro, D. M.; Jenkins, D. M.; Iavarone, A. T.; Glover, S. D.; Kubiak, C. P.; Long, J. R. High-Spin Ground States via Electron Delocalization in Mixed-Valence Imidazolate-Bridged Divanadium Complexes. *Nat. Chem.* **2010**, *2* (5), 362–368.
(49) Sun, Y.; Bigi, J. P.; Piro, N. A.; Tang, M. L.; Long, J. R.; Chang, C. J. Molecular Cobalt Pentapyridine Catalysts for Generating Hydrogen from Water. *J. Am. Chem. Soc.* **2011**, *133* (24), 9212–9215.
(50) Karunadasa, H. I.; Montalvo, E.; Sun, Y.; Majda, M.; Long, J. R.; Chang, C. J. A Molecular MoS2 Edge Site Mimic for Catalytic Hydrogen Generation. *Science* **2012**, *335* (6069), 698–702.
(51) Chantarojsiri, T.; Sun, Y.; Long, J. R.; Chang, C. J. Water-Soluble Iron(IV)-Oxo Complexes Supported by Pentapyridine Ligands: Axial Ligand Effects on Hydrogen Atom and Oxygen Atom Transfer Reactivity. *Inorg. Chem.* **2015**, *54* (12), 5879–

5887.
(52) Zee, D. Z.; Chantarojsiri, T.; Long, J. R.; Chang, C. J. Metal-Polypyridyl Catalysts for Electro- and Photochemical Reduction of Water to Hydrogen. *Acc. Chem. Res.* **2015**, *48* (7), 2027–2036.
(53) Savéant, J.-M.; Costentin, C. *Elements of Molecular and Biomolecular Electrochemistry: An Electrochemical Approach to Electron Transfer Chemistry*, 2nd ed.; John Wiley & Sons: Hoboken, 2019.
(54) Nadjo, L.; Savéant, J. M.; Su, K. B. Homogeneous Redox Catalysis of Multielectron Electrochemical Reactions. Part II. Competition between Homogeneous Electron Transfer and Addition on the Catalyst. *J. Electroanal. Chem.* **1985**, *196* (1), 23–34.
(55) Andrieux, C. P.; Gallardo, I.; Savéant, J. M.; Su, K. B. Dissociative Electron Transfer. Homogeneous and Heterogeneous Reductive Cleavage of the Carbon-Halogen Bond in Simple Aliphatic Halides. *J. Am. Chem. Soc.* **1986**, *108* (4), 638–647.
(56) Biddulph, M. A.; Davis, R.; Wells, C. H. J.; Wilson, F. I. C. Reactions between Dinuclear Metal Carbonyl Complexes and Alkyl Halides: Formal Oxidative Addition across a Metal-Metal Single Bond. *J. Chem. Soc. Chem. Commun.* **1985**, No. 19, 1287–1288.
(57) Herrick, R. S.; Herrinton, T. R.; Walker, H. W.; Brown, T. L. Rates of Halogen Atom Transfer to Manganese Carbonyl Radicals. *Organometallics* **1985**, *4* (1), 42–45.
(58) Halpern, J.; Maher, J. P. Kinetics of the Reactions of Pentacyanocobaltate(II) with Organic Halides. *J. Am. Chem. Soc.* **1965**, *87* (23), 5361–5366.
(59) Marcus, R. A. The Second R. A. Robinson Memorial Lecture: Electron, Proton and Related Transfers. *Faraday Discuss. Chem. Soc.* **1982**, *74* (0), 7–15.
(60) Hush, N. S. Adiabatic Rate Processes at Electrodes. I. Energy-Charge Relationships. *J. Chem. Phys.* **1958**, *28* (5), 962–972.
(61) Marcus, R. A. On the Theory of Oxidation-Reduction Reactions Involving Electron Transfer. I. *J. Chem. Phys.* **1956**, *24* (5), 966–978.
(62) Lexa, D.; Mispelter, J.; Savéant, J. M. Electroreductive Alkylation of Iron in Porphyrin Complexes. Electrochemical and Spectral Characteristics of σ-Alkyliron Porphyrins. *J. Am. Chem. Soc.* **1981**, *103* (23), 6806–6812.
(63) Barnes, J. T.; Griffith, K. J.; Beeler, J. A.; Gerroll, B. H. R.; Couto Petro, A. G.; Williams, C. G.; Siedle, A. R.; Tait, S. L.; Peters, D. G. Alkyl-Group Grafting onto Glassy Carbon Cathodes by Reduction of Primary Monohaloalkanes: Electrochemistry and X-Ray Photoelectron Spectroscopy Studies. *J. Electroanal. Chem.* **2020**, *856*, 113531.
(64) Savéant, J. M.; Su, K. B. Homogeneous Redox Catalysis of Electrochemical Reaction. Part VI. Zone Diagram Representation of the Kinetic Regimes. *J. Electroanal. Chem.* **1984**, *171* (1–2), 341–349.
(65) Lai, D.; Griller, D.; Husband, S.; Ingold, K. U. Kinetic Applications of Electron Paramagnetic Resonance Spectroscopy. XVI. Cyclization of the 5-Hexenyl Radical. *J. Am. Chem. Soc.* **1974**, *96* (20), 6355–6357.
(66) Andrieux, C. P.; Savéant, J. M.; Gallardo, I. Outer-Sphere Electron-Transfer Reduction of Alkyl Halides. A Source of Alkyl Radicals or of Carbanions? Reduction of Alkyl Radicals. *J. Am. Chem. Soc.* **1989**, *111* (5), 1620–1626.
(67) Alender, J.; Morgan, P.; Timberlake, J. Decomposition of N,N-Dialkylthiadiaziridine 1,1-Dioxides: A Mechanistic Revision. *J. Org. Chem.* **1983**, *48* (5), 755–756.
(68) Murakami, Y.; Hisaeda, Y.; Fan, S.-D. Characterization of a Simple Vitamin B 12 Model Complex and Its Catalysis in Electrochemical Carbon-Skeleton Rearrangement . *Chem. Lett.* **1987**, *16* (4), 655–658.
(69) James H.P. Utley; Little, R. D.; Nielsen, M. F. Reductive Coupling. In *Organic Electrochemistry*; Hammerich, O., Speiser, B., Eds.; CRC Press: Boca Raton, 2015; pp 621–704.
(70) Salamone, M.; Milan, M.; Dilabio, G. A.; Bietti, M. Reactions of the Cumyloxyl and Benzyloxyl Radicals with Tertiary Amides. Hydrogen Abstraction Selectivity and the Role of Specific Substrate-Radical Hydrogen Bonding. *J. Org. Chem.* **2013**, *78* (12), 5909–5917.
(71) Studer, A.; Curran, D. P. Catalysis of Radical Reactions: A Radical Chemistry Perspective. *Angew. Chem. Int. Ed.* **2016**, *55* (1), 58–102.
(72) Curran, D. P.; Kim, D. Atom Transfer Cyclization of Simple Hexenyl Iodides. A Caution on the Use of Alkenyl Iodides as Probes for the Detection of Single Electron Transfer Processes. *Tetrahedron Lett.* **1986**, *27* (48), 5821–5824.
(73) Ramprasad, D.; Gilicinski, A. G.; Markley, T. J.; Pez, G. P. Cobalt(II) Polypyridine Complexes and Their Reversible Reactivity with Dioxygen. *Inorg. Chem.* **1994**, *33* (13), 2841–2847.
(74) Andrieux, C. P.; Blocman, C.; Dumas-Bouchiat, J. M.; M'Halla, F.; Savéant, J. M. Homogeneous Redox Catalysis of Electrochemical Reactions. Part V. Cyclic Voltammetry. *J. Electroanal. Chem.* **1980**, *113* (1), 19–40.
(75) Jones, G. D.; Martin, J. L.; McFarland, C.; Allen, O. R.; Hall, R. E.; Haley, A. D.; Brandon, R. J.; Konovalova, T.; Desrochers, P. J.; Pulay, P.; et al. Ligand Redox Effects in the Synthesis, Electronic Structure, and Reactivity of an Alkyl-Alkyl Cross-Coupling Catalyst. *J. Am. Chem. Soc.* **2006**, *128* (40), 13175–13183.
(76) Scarborough, C. C.; Lancaster, K. M.; Debeer, S.; Weyhermüller, T.; Sproules, S.; Wieghardt, K. Experimental Fingerprints for Redox-Active Terpyridine in [Cr(Tpy) 2](PF 6) n (n = 3-0), and the Remarkable Electronic Structure of [Cr(Tpy) 2] 1-. *Inorg. Chem.* **2012**, *51* (6), 3718–3732.
(77) Hupp, J. T.; Weaver, M. J. Prediction of Electron-Transfer Reactivities from Contemporary Theory: Unified Comparisons for Electrochemical and Homogeneous Reactions. *J. Phys. Chem.* **1985**, *89* (13), 2795–2804.
(78) Anderson, T. J.; Jones, G. D.; Vicic, D. A. Evidence for a NiI Active Species in the Catalytic Cross-Coupling of Alkyl Electrophiles. *J. Am. Chem. Soc.* **2004**, *126* (26), 8100–8101.
(79) Lin, X.; Phillips, D. L. Density Functional Theory Studies of Negishi Alkyl-Alkyl Cross-Coupling Reactions Catalyzed by a Methylterpyridyl-Ni(I) Complex. *J. Org. Chem.* **2008**, *73* (10), 3680–3688.
(80) Costentin, C.; Drouet, S.; Robert, M.; Savéant, J.-M. A Local Proton Source Enhances CO2 Electroreduction to CO by a Molecular Fe Catalyst. *Science* **2012**, *338* (6103), 90–94.
(81) Costentin, C.; Savéant, J. M.; Tard, C. Ligand "Noninnocence" in Coordination Complexes vs. Kinetic, Mechanistic, and Selectivity Issues in Electrochemical Catalysis. *Proc. Natl. Acad. Sci. U. S. A.* **2018**, *115* (37), 9104–9109.

Table of Contents

Divergent Radical Pathways via Metal-Ligand Cooperativity